ACS NANO
Cite This: ACS Nano 2018, 12, 10797−10806
www.acsnano.org

ARTICLE

In Situ SiRNA Assembly in Living Cells for Gene Therapy with MicroRNA Triggered Cascade Reactions Templated by Nucleic Acids

Kewei Ren,[†,§] Yue Zhang,[†,§] Xiaobo Zhang,[†] Ying Liu,[*,†] Min Yang,[‡] and Huangxian Ju[*,†]

[†]State Key Laboratory of Analytical Chemistry for Life Science, School of Chemistry and Chemical Engineering, Nanjing University, Nanjing 210023, P. R. China

[‡]Department of Pharmaceutical and Biological Chemistry, UCL School of Pharmacy, University College London, London WC1N 1AX, United Kingdom

Supporting Information

ABSTRACT: **The *in situ* generation of siRNAs in living cells can greatly enhance the specificity and efficiency of gene therapy. Inspired by the natural molecular machines that organize different compartments sequentially in a limited space to facilitate cellular process, this work constructs a DNA nanomachine (DNM) by alternately hybridizing two pairs of DNA/RNA hybrids to a DNA scaffold generated by rolling circle amplification for highly efficient *in situ* siRNA assembly in living cells. After target cell-specific delivery of DNM, intracellular specific microRNA can work as a trigger to operate the DNM by initiating DNA cascade displacement reaction between DNA/RNA hybrids along the scaffold for continuous generation of siRNAs. Using miR-21 as a model, efficient siRNAs generation is achieved *via* DNA templated cascade reaction, which demonstrated impressive suppressions to VEGF mRNA and protein expressions in cells and *in vivo* tumor growth and indicated promising application of the designed strategy in gene therapy.**

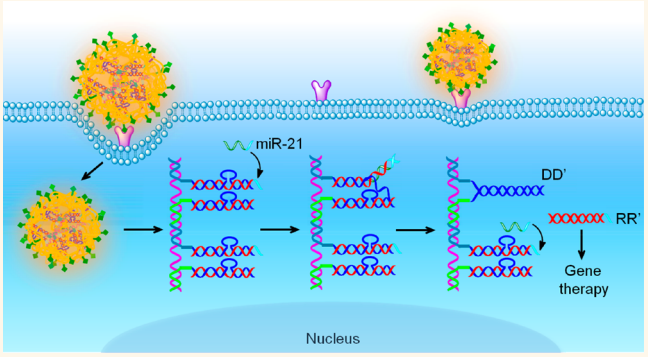

KEYWORDS: *DNA nanomachine, siRNA generation, DNA templated cascade reaction, microRNA, gene interference*

Synthetic small interfering RNAs (siRNAs), which can intracellularly silence disease-causing genes, have been used as a class of medicines to treat cancers and a wide range of diseases such as amyotrophic lateral sclerosis, Huntington's disease (HD), Alzheimer's disease (AD), and Parkinson's disease (PD).[1−4] One of the biggest challenges in RNA interfering (RNAi)-based therapeutics is delivering the synthetic siRNAs into cells due to their cell impermeability and susceptibility to degradations.[5−7] Although a variety of nanoparticles, polymers, and DNA structures have been used as carriers for siRNA delivery,[8−12] the unavoidable leakage of *in vitro* synthesized siRNA and uncontrollable degradation as well as "off-target" toxicity diminish gene therapy efficiency.[13,14] Therefore, *in situ* generation of siRNA in target cells is an appropriate approach to enhance the specificity and efficiency of gene therapy, and several DNA/RNA hybridization/displacement reactions have been applied in living cells to *in situ* generate siRNA for gene therapies.[15,16] However, the assembly efficiencies of current intracellular siRNA generation approaches through the spontaneous collisions of two DNA/RNA hybrids in molecularly crowded intracellular environment are limited due to the lack of controllability and the low reaction rates.[15] Developing a controlled siRNA assembly system with high reaction efficiency in dynamically changing cytoplasm is of great significance to precise gene therapy.[17,18]

The naturally occurring intracellular synthesis relies on natural molecular machines that can organize different compartments sequentially in a limited space to carry out machinery work in tandem with one another to facilitate reaction process.[19−21] A large number of natural intracellular molecular machines are composed of nucleic acid scaffolds such as transposons, spliceosomes, and ribosomes, which offer high reaction efficiency and specificity due to Watson−Crick base pairing.[22,23] Inspired by the natural nucleic acid templated synthesis, programmable DNA nanostructures have been applied *in vitro* to assist cascade enzymatic reactions by substrate channeling[24,25] and cofactor[26] as well as to guide sequence-defined polymer and peptide synthesis.[27−30] The

Received: March 30, 2018
Accepted: October 12, 2018
Published: October 12, 2018

DOI: 10.1021/acsnano.8b02403
ACS Nano 2018, 12, 10797−10806

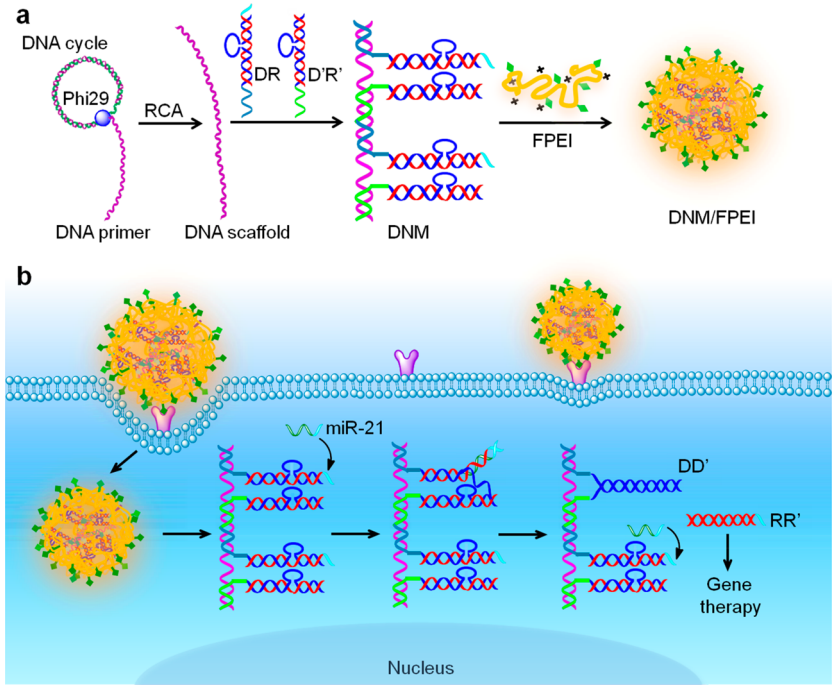

Figure 1. Schematic illustration of intracellular siRNA cascade assembly with a microRNA-triggered DNM in living cells. (a) Synthesis of DNM and DNM/FPEI and (b) target cell-specific delivery of DNM/FPEI for miR-21 triggered assembly of siRNA in living cells.

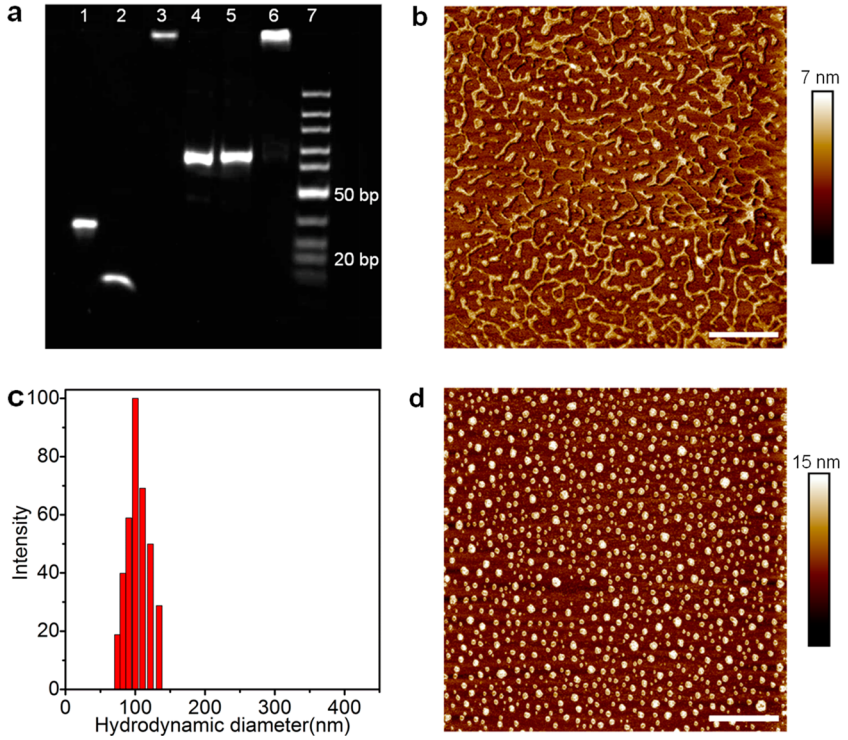

Figure 2. Characterization of DNM and DNM/FPEI nanocomposites. (a) PAGE analysis of DNA primer, DNA cycle, DNA scaffold, DR, D′R′, DNM, and DNA ladder marker (lanes 1−7). (b) AFM phase image of DNM. Scale bar: 200 nm. (c) Hydrodynamic diameter distribution of DNM/FPEI. (d) AFM phase image of DNM/FPEI. Scale bar: 800 nm.

nucleic acid templated small reaction area confines free diffusion of reactants and enhances their local concentrations, which can accelerate the reaction and greatly improve reaction efficiency.[31,32] However, the application of DNA templated synthetic reactions has not been extended into living cells due to the involvement of exotic enzymes and catalyst.

Here we designed a strategy for *in situ* assembly of siRNA in living cells *via* microRNA (miRNA or miR) driving cascade reaction in a DNA nanomachine (DNM). The DNM was constructed by alternately hybridizing two pairs of DNA/RNA hybrids (DR and D′R′) to a DNA scaffold. The proximity and precise arrangement of DR and D′R′ along the scaffold

DOI: 10.1021/acsnano.8b02403
ACS Nano 2018, 12, 10797−10806

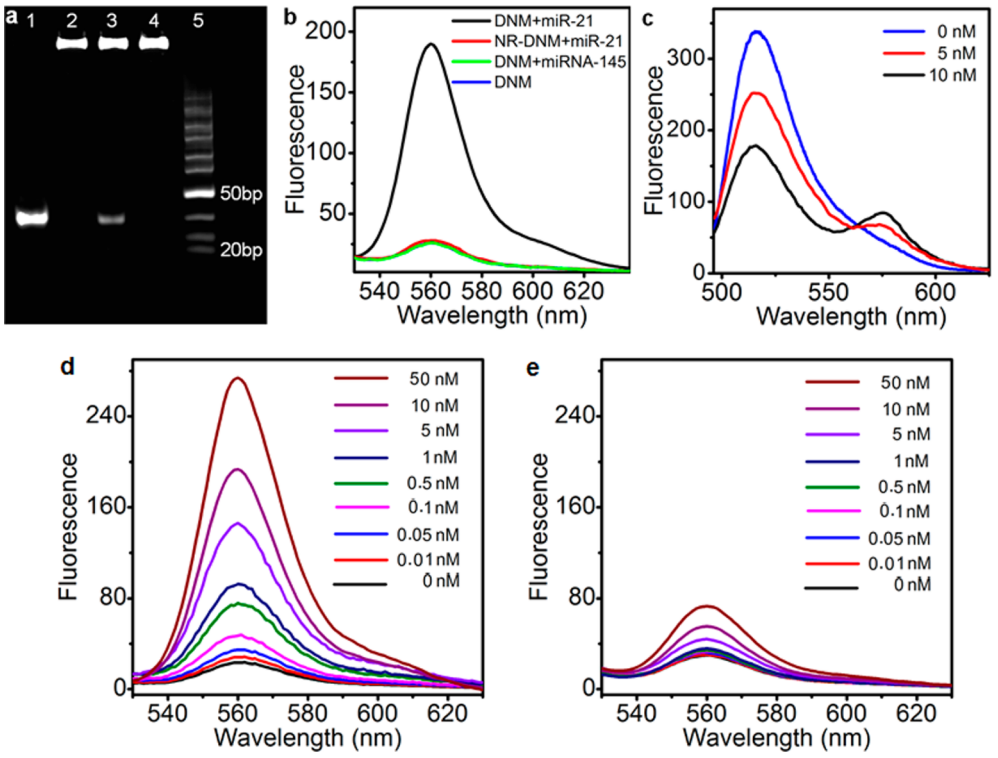

Figure 3. Characterization of siRNA generation with miRNA-triggered DNM. (a) PAGE image of (1) 5 μM RR′, (2) 2 μM DNM, (3) mixture of 2 μM DNM and 10 nM miR-21, (4) mixture of 2 μM DNM and 10 nM control miRNA, and (5) 2 μM DNA ladder marker. (b) Fluorescence spectra of SQ-DNM (DNM) and SQ-DNM in response to 10 nM miR-21 (DNM + miR-21) and 10 nM miR-145 (DNM + miR-145) at λ_{ex} of 510 nm, and SQ-NR-DNM in response to 10 nM miR-21 (NR-DNM + miR-21). (c) Fluorescence spectra of bicolor DNM prepared with FAM-R and TAMRA-R′ at λ_{ex} of 480 nm in response to 5 nM and 10 nM miR-21. Fluorescence spectra of (d) SQ-DNM and (e) the mixture of SQ-DR and D′R′ after incubated with miR-21 at various concentrations for 60 min.

guaranteed high reaction efficiency for intracellular siRNA generation.[33,34] Using miR-21 as the specific model trigger to operate the DNA cascade strand displacement reaction in DNM, the continuous generation of siRNA proceeded along the DNA scaffold, which was precisely controllable in time and space. The highly efficient gene silencing to suppress mRNA and protein expressions in cells and *in vivo* tumor growth demonstrated the practicability of this approach in gene therapy. Compared with the conventional gene interference technology,[35,36] the miR-21-triggered intracellular siRNA assembly with nucleic acids templated cascade reactions provides higher therapeutic specificity than that directly delivers siRNA into cells and improves delivery stability by substituting the duplex siRNA with DNM. The high biocompatibility, impressive controllability, and reaction efficiency of miR-21-triggered DNM could be further extended to *in situ* generation and biosensing of other nucleic acids and biomolecules.

RESULTS AND DISCUSSION

Principle of Intracellular SiRNA Assembly with MiRNA-Triggered DNM. As shown in Figure 1a, the DNA/RNA hybrids (DR and D′R′) were alternatively arranged on a DNA scaffold, which was previously produced by rolling circle amplification (RCA), to form DNM. DR and D′R′ were synthesized by hybridizing ssDNA (D or D′) with specific RNA (R or R′), respectively, which formed two complementary bulge loop conformations.[37,38] Here the 5′ end of R is labeled with Cy3 (Cy3-R) for *in situ* monitoring the cellular process, and its 3′ end has a toehold complementary to 5′ end of specific miRNA.[39] The negatively charged DNM could form a stable nanocomposite with cationic folic acid modified polyethylenimine (FPEI) to facilitate target cell-specific delivery and assist the endosomal escape of DNM into the cytoplasm.[40] Afterward, intracellular specific miRNA could recognize the toehold of R and hybridize with the first 22 nucleotides of R starting from the 3′-end to open the bulge loop of DR. The released bulge loop of D worked as an activated toehold to react with the bulge loop of D′ subsequently, which triggered the strand displacement reaction between DR and D′R′ to generate dsDNA (DD′) on the DNA scaffold and release both the siRNA (RR′) and the miRNA from the DNM.[16,38] The released miRNA triggered the next strand displacement reaction between DR and D′R′ for continuously generating siRNA in living cells (Figure 1b).

Characterization of DNM and DNM/FPEI. The synthesis of DNM was demonstrated by polyacrylamide gel electrophoresis (PAGE) analysis (Figure 2a). The RCA product showed a band with much lower mobility (lane 3) than DNA primer and DNA cycle (lanes 1 and 2), while the hybridization mixture showed only one band with much lower mobility (lane 6) than DR and D′R′ (lanes 4 and 5), suggesting the formation of DNA scaffold and the successful synthesis of DNM. Both the products of RCA and DNM barely moved in polyacrylamide gels due to their large molecular masses and sizes.[41,42] Atomic force microscopic (AFM) image of DNM demonstrated monodispersed branch-like structure with an average length of 250 ± 100 nm (Figure 2b). Considering the 48-base length of DNA cycle (16 nm)[43] for forming the repeated sequences to hybridize DR and D′R′, the DNM

DOI: 10.1021/acsnano.8b02403
ACS Nano 2018, 12, 10797−10806

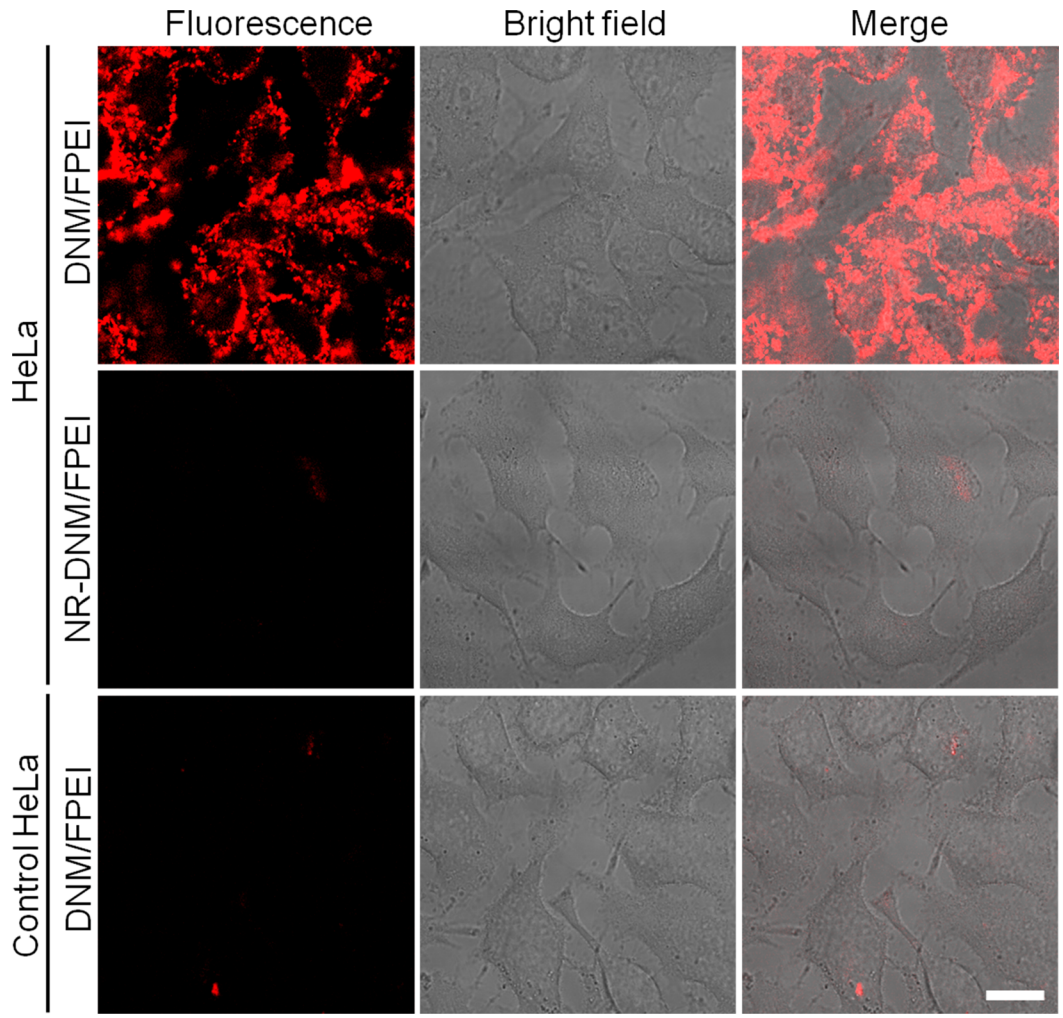

Figure 4. Characterization of siRNA cascade generation with miRNA-triggered DNM in HeLa cells. Confocal fluorescence images of HeLa cells incubated with SQ-DNM/FPEI, SQ-NR-DNM/FPEI, and antisense miR-21 treated HeLa cells (control HeLa) incubated with SQ-DNM/FPEI as control. Scale bar: 20 μm.

contained 16 ± 6 pairs of DR/D′R′. To further confirm the number, aminomethylcoumarin (AMCA)-labeled DNA primer, Cy3-R, and Cy5-labeled R′ were used to synthesize the tricolor DNM. From the fluorescence signals of AMCA, Cy3, and Cy5 in the DNM, the ratios of DNM: DR: D′R′ were about 1:16.9:17.0 (Figure S1), which was consistent with the AFM result.

To evaluate the performances and applications of DNM, self-quenched DR (SQ-DR) was prepared with Cy3-R and corresponding quencher BHQ2-labeled D to synthesize a self-quenched DNM (SQ-DNM). Upon addition of 10% fetal bovine serum, the fluorescence recovery of free SQ-DR was much greater than the SQ-DNM (Figure S2a), suggesting that DNM provided good protection of DR against nuclease degradation. The melting temperature (T_m) of 77.6 °C indicated good thermal stability of the DNM (Figure S2b and S2c).

The synthetic FPEI was verified with its ^{1}HNMR spectrum and the UV−vis and FTIR spectra of FPEI, PEI, and FA (Figure S3). Zeta potential analysis also confirmed the formation of DNM/FPEI (Figure S4), and the FPEI wrapping effectively compressed the size of DNM to around 100 nm (Figure 2c and 2d), which is more appropriate for cellular internalization.[44,45]

Feasibility of SiRNA Assembly with MiRNA-Triggered DNM. The feasibility of miR-21 as a trigger to specifically initiate cascade strand displacement reaction in DNM for *in situ* siRNA generation was first verified *via* PAGE analysis (Figure 3a). After incubating 2 μM DNM with 10 nM miR-21, a band representing RR′ (lane 1) appeared (lane 3), indicating the successful generation of siRNA. The assembly efficiency was calculated from the intensity of the generated siRNA band, which was about 58.5% with the DNM/miR-21 molar ratio of 200, indicating the high siRNA generation efficiency. Incubating DNM with control miRNA (miR-145) did not yield any new band (lanes 4), demonstrating the high specificity of miRNA-triggered cascade strand displacement reaction. The strong fluorescence of Cy3 could be observed from SQ-DNM in the presence of miR-21 due to the formation of BHQ2-DD′ on the DNM and release of Cy3-RR′, while it was very weak in the mixtures of miR-145 with SQ-DNM or the mixture of miR-21 with SQ-NR-DNM that was not responsive to miR-21 (Figure 3b), further confirming the reaction specificity of miR-21-triggered cascade strand displacement reaction between DR and D′R′. The specificity of DNM in response to miR-21 for siRNA generation was also demonstrated by comparing the responses of DNM to single-base mismatched miR-21, three-base mismatched miR-21, and

DOI: 10.1021/acsnano.8b02403
ACS Nano 2018, 12, 10797−10806

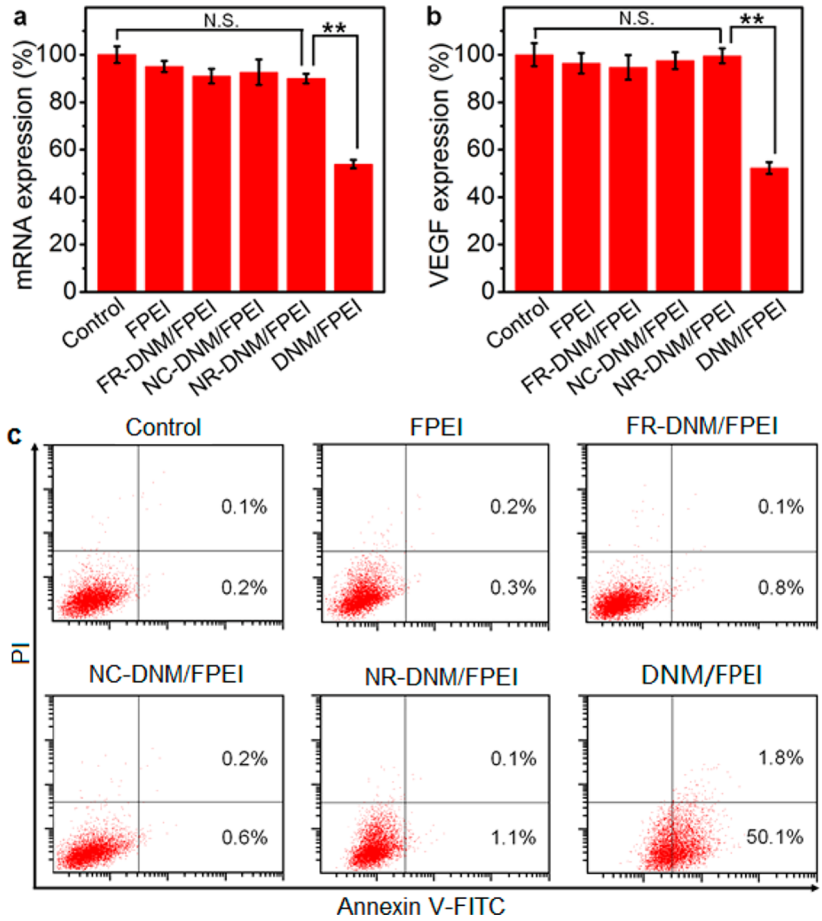

Figure 5. Intracellular therapeutic effect of miRNA-triggered DNM. (a) Real-time PCR characterization of VEGF mRNA expression and (b) ELISA characterization of protein expression in HeLa cells and (c) apoptosis of HeLa cells after incubated with 100 nM FPEI, FR-DNM/FPEI, NC-DNM/FPEI, NR-DNM/FPEI, and DNM/FPEI for 3 h and then incubated in DMEM for 48 h at 37 °C, and HeLa cells without any treatment as control. The data error bars indicate means ± SD (n = 3). **P < 0.01 (two-tailed Student's t test). The cell apoptosis is tested with Annexin V-FITC/PI apoptotic kit.

miR-145 (Figure S5). The formation of RR′ was also demonstrated by the FRET signal of tetramethylrhodamine (TAMRA)-labeled R′ from bicolor DNM prepared with 5-carboxyfluorescein (FAM)-labeled R and TAMRA-labeled R′ after incubated with miR-21 (Figure 3c). Moreover, this signal was positively depended on miR-21 concentration.

To demonstrate the effect of interval distance between DR and D′R′ in DNM on the efficiency of siRNA generation, a series of DNMs with different base numbers between DR and D′R′ were prepared. In the presence of 10 nM miR-21, the highest siRNA generation efficiency indicated by the fluorescence intensity was achieved at 8-bases distance (Figure S6). Hence, the DNM with 8-bases distance between DR and D′R′ was used for subsequent experiments.

The kinetics for siRNA assembly *via* miRNA-triggered cascade strand displacement reaction of DR and D′R′ in DNM was much quicker than that *via* random strand displacement reaction of DR and D′R′ in homogeneous solution in the presence of miRNA (Figure S7). The former could reach the maximum generation in 16 min, while the latter reached an equilibrium at 80 min, demonstrating the substantial acceleration and highly efficient generation of siRNA.

To demonstrate the high efficiency of siRNA generation *via* miR-21-triggered DNM, the yield of siRNA from DNM was evaluated *in vitro* at different miR-21 concentrations by measuring Cy3 fluorescence recovery from SQ-DNM, which increased with the increasing miR-21 concentration (Figure 3d). At the reaction time of 60 min and the same miR-21 concentrations, the formed RR′ showed much stronger fluorescence of Cy3 than that from the reaction of DR and D′R′ in homogeneous solution (Figure 3e). The Cy3 fluorescence of SQ-DNM in response to 50.0 pM miR-21 was 12.4-times stronger than that from the mixture of SQ-DR and D′R′, indicating the high efficiency of siRNA generation.

Intracellular SiRNA Assembly with MiRNA-Triggered DNM. The feasibility of intracellular siRNA generation from DNM was demonstrated with miR-21 and HeLa cells as model. After the cells were transfected with SQ-DNM/FPEI, Cy3 fluorescence in response to intracellular miR-21 was clearly observed (Figure 4), indicating the successful intracellular generation of siRNA. The nuclear localization images demonstrated complete fluorescence separation of 4′,6-diamidino-2-phenylindole (DAPI) in nuclear from Cy3 in cytoplasm (Figure S9), indicating that the siRNA generation proceeded in cytoplasm. Here, the inhomogeneous intracellular fluorescence was attributed to the distribution of miR-21 in cytoplasm, which was infected by the inhomogeneous cellular environment. The fluorescence signal of Cy3 in Z-stack images exhibited a position-sensitive dependence,[46] demonstrating intracellular localization of the generated siRNA

DOI: 10.1021/acsnano.8b02403
ACS Nano 2018, 12, 10797−10806

(Figure S8). As control, the treatment of HeLa cells with SQ-NR-DNM/FPEI showed little intracellular fluorescence (Figure 4), indicating the specificity of miR-21 initiated intracellular siRNA generation. Furthermore, after the cells were treated with synthetic miR-21 antisense strands (anti-miR-21) to entirely suppress miR-21 expression (Figure S10) and then transfected with SQ-DNM/FPEI, they generated little Cy3 fluorescence (Figure 4). Flow cytometric assay showed the same results (Figure S11). The bicolor DNM labeled with FAM and TAMRA further confirmed the response specificity. After it was wrapped with FPEI and delivered into HeLa cells, successful intracellular FRET process was achieved between FAM and TRAMA upon the generation of siRNA, and only FAM fluorescence was observed when HeLa cells were incubated with bicolor NR-DNM/FPEI or miR-21 expression-suppressed HeLa cells were incubated with bicolor DNM/FPEI (Figure S12). The intense FRET signal upon the operation of DNM *via* miR-21 activation in HeLa cells eliminated the false-positive signal from thermodynamic fluctuations and chemical interferences (such as nuclease and glutathione),[47] thus confirming the successful intracellular generation of siRNA.

The specific cell transfection of DNM/FPEI was achieved by folic acid (FA) receptor-mediated cell endocytosis, which was demonstrated by the much lower fluorescence recovery of Cy3 after the cells were incubated with SQ-DNM/PEI than that from SQ-DNM/FPEI transfected cells (DNM/PEI, DNM/FPEI, Figure S13). The internalization of SQ-DNM/FPEI could be highly suppressed for the cells previously treated with excessive FA (FA+DNM/FPEI, Figure S13), proving that FA played important roles in the targeted delivery of DNM/FPEI to HeLa cells.[48] The transfection specificity was further verified by the negligible Cy3 fluorescence from the FA receptor-negative human epidermal HaCat cells after treated with SQ-DNM/FPEI (Figure S14).

To unequivocally evaluate the internalization pathway of the DNM/FPEI into the cells, a series of inhibitors including NaN_3, wortmannin, genistein, and sucrose were used to selectively block different cellular uptake processes (Figure S15). An obvious decrease in cellular uptake was observed when the cells were incubated with NaN_3, indicating the energy-dependent internalization of DNM/FPEI.[49] Moreover, the cells treated with genistein and sucrose caused 40−50% reduction in DNM/FPEI uptake, suggesting that DNM/FPEI experienced the caveole- and clathrin-dependent endocytosis pathways upon entering the cells.[50]

Gene Silencing and Cell Apoptosis Assays. Vascular endothelial growth factor (VEGF) was selected as a model target to evaluate the therapeutic effect of *in situ* siRNA generation. After HeLa cells were incubated with 100 nM DNM/FPEI for 3 h and cultured in culture medium for 48 h, the intracellular generation of siRNA effectively suppressed VEGF mRNA expression by 46.1% and VEGF protein expression by 47.3% due to the gene silencing. The control experiments using FPEI, NR-DNM/FPEI, and FR-DNM/FPEI that could not perform strand displacement reaction to generate siRNA and NC-DNM/FPEI that could generate a negative control siRNA in the presence of miR-21 to transfect the HeLa cells showed little inhibition to VEGF mRNA expression and protein synthesis (Figure 5a and 5b). These results demonstrated the *in situ*-specific formation of VEGF-related siRNA in HeLa cells.

MTT assay showed the inhibition effect of DNM/FPEI to HeLa cell proliferation. After HeLa cells were treated with DNM/FPEI for 3 h and cultured in DMEM for 48 h, the cell proliferation obviously decreased in comparison to the untreated cells as control and the cells treated with FPEI, FR-DNM/FPEI, NC-DNM/FPEI, and NR-DNM/FPEI (Figure S16). The latter ones did not show the inhibition effect. Moreover, the inhibition effect was dose dependent, and the cell proliferation percentage decreased to 42.1% at 100 nM DNM/FPEI. To evaluate the therapeutic effect of DNM/FPEI, the cell apoptosis was monitored with flow cytometry and Annexin V-FITC/PI apoptosis kit. The total apoptosis rate for DNM/FPEI treated cells was 50.1%, while FPEI, FR-DNM/FPEI, NC-DNM/FPEI, and NR-DNM/FPEI treated cells showed negligible apoptosis (Figure 5c), indicating that the *in situ* siRNA generation from DNM was a promising strategy for cancer gene therapy.

The high intracellular siRNA generation efficiency templated by nucleic acids to enhance the therapeutic effect was demonstrated by delivering SQ-DNM (DNM/Lipo) or the mixture of 100 nM SQ-DR and D′R′ ((DR + D′R′)/Lipo) into HeLa cells. Here Lipofectamine 2000 was used to transfect DNM or the mixture for avoiding the effect of strand length of transfected nucleic acids on transfection efficiency of PEI.[44] In comparison with (DR + D′R′)/Lipo, DNM/Lipo showed higher efficiencies for inhibiting VEGF mRNA and protein expressions (44.2% and 42.6%, respectively), restraining cell proliferation (40.4%) and inducing apoptosis (40.8%) (Figure S17), indicating the better therapeutic effect of DNM/FPEI than DNM/Lipo and the significant advantages of DNM assembly.

HepG2 cells were chosen to investigate the applicability of DNM/FPEI-based siRNA therapy to other cancer cells. The bright fluorescence of Cy3 was observed in HepG2 cells treated with SQ-DNM/FPEI, indicating the successful intracellular generation of siRNA (Figure S18a), which was also verified by flow cytometric assay (Figure S18b). The VEGF mRNA and VEGF protein expressions in HepG2 cells treated with 100 nM DNM/FPEI were inhibited by about 46.0% and 49.7%, respectively (Figure S19a and S19b), and the cell proliferation decreased to 57.0% along with the raised apoptosis rate of 56.5% compared with the untreated cells and the cells treated with NC-DNM/FPEI (Figure S19c and S19d), indicating the potential therapeutic effect for various cancer types.

***In Vivo* Therapeutic Applicability.** The antitumor efficacy of DNM *via* inhibition of VEGF expression from *in vivo* generated siRNA was investigated with mice bearing HeLa xenograft tumors. DNM/FPEI, NC-DNM/FPEI, and NR-DNM/FPEI were intravenously injected into these mice every 2 days, respectively, and the inhibition efficacy toward tumor growth was monitored. DNM/FPEI presented effective inhibition efficacy toward tumor growth, while no therapeutic effect was observed for NC-DNM/FPEI and NR-DNM/FPEI treated mice compared with the control mice group (PBS injected) (Figure 6), indicating very high antitumor efficacy of DNM/FPEI. During the experiment period of 14 days, these mice did not show obvious variation in their body weights (Figure S19), indicating the satisfactory biocompatibility of DNM/FPEI. Thus, *in situ* siRNA generation with DNM was a promising approach for highly efficient cancer therapy.

DOI: 10.1021/acsnano.8b02403
ACS Nano 2018, 12, 10797−10806

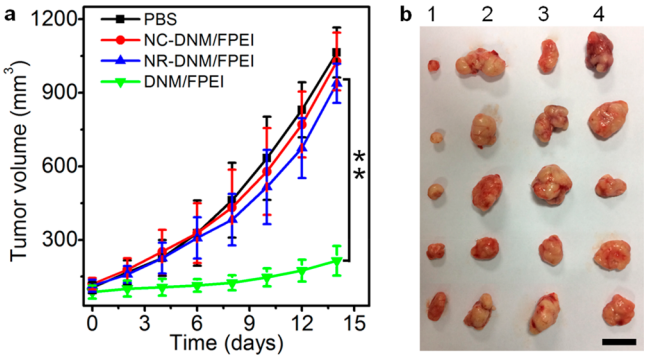

Figure 6. *In vivo* demonstration of therapeutic applicability of miRNA-triggered DNM. (a) Tumor volumes of mice groups with intravenous injection of different nanocomposites every 2 days. Error bars indicate means ± SD (n = 5). **P < 0.01 (two-tailed Student's t test). (b) Representative images of HeLa tumors collected from (1) DNM/FPEI, (2) NR-DNM/FPEI, (3) NC-DNM/FPEI, and (4) PBS injected mice groups at day 14. Scale bar: 1 cm.

CONCLUSIONS

This work designs a miRNA triggered DNM to *in situ* assemble siRNA *via* cascade strand displacement reaction in cells. The highly efficient siRNA generation shows great suppression to miRNA-specific mRNA expression and protein synthesis in living cells. The DNM can be conveniently synthesized *via* alternately hybridizing two pairs of DNA/RNA hybrids to a DNA scaffold generated by rolling circle amplification and shows satisfactory biocompatibility and good stability. Upon miRNA triggering, specific siRNA can be continuously assembled along the scaffold in a relatively short time due to the confined reaction area, which provides high reaction efficiency. Using VEGF as a model target, the continuously assembled siRNA *via* nucleic acids template can efficiently inhibit the proliferation of HeLa cells and the growth of HeLa xenograft tumor and shows exciting antitumor efficacy. This strategy can be easily extended for *in situ* generation of other genes by changing the corresponding hybrid pairs, thus possesses promising application in biosensing and precise gene therapy.

METHODS

Reagents. Phi29 DNA polymerase, T4 DNA ligase, exonuclease I, exonuclease III, and dNTPs were purchased from New England Biolabs Ltd. Human VEGF ELISA kit and Annexin V-FITC apoptosis detection kit were purchased from BD Biosciences (USA). DNA purification kit was obtained from ComWin Biotech Co., Ltd. (China). DAPI was purchased from KeyGEN Biotech (China). Lipofectamine 2000 was purchased from ThermoFisher scientific (USA). Linear polyethylenimine (PEI, 25,000), folic acid (FA), *N*-hydroxysuccinimide (NHS), and *N*-(3-dimethylamino propyl-*N*′-ethylcar-bodiimide) hydrochloride (EDC·HCl) were purchased from Sigma-Aldrich (USA). Phosphate buffer saline (PBS, pH 7.4) contained 136.7 mM NaCl, 2.7 mM KCl, 8.72 mM Na_2HPO_4, and 1.41 mM KH_2PO_4. All other reagents were of analytical grade. All aqueous solutions were prepared using ultrapure water (≥18 MΩ, Milli-Q, Millipore). RNAs were obtained from GenePharma Co. Ltd. (Shanghai, China). The RNA sequences were as follows:

VEGF RNA, sense:

Cy3-R, 5′-Cy3-GGAGUACCCUGAUGAGAUCAACAUCAGUCUGAUAAGCUA-3′

FAM-R, 5′-FAM-GGAGUACCCUGAUGAGAUCAACAUCAGUCUGAUAAGCUA-3′

Cy3-NR, 5′-Cy3-GGAGUACCCUGAUGAGAUCAACAUCAGUCUGA-3′

FAM-NR, 5′-FAM-GGAGUACCCUGAUGAGA UCAACAUCAGUCUGA-3′

VEGF RNA, antisense:

R′, 5′-UCAGACUGAUGUUGAUCUCAUCAGGGUACUCCGG-3′

TAMRA-R′, 5′-UCAGACUGAUGUUGAUCUCAUCAGGGU ACUCCGG-TAMRA-3′

negative control RNA, sense:

5′-UUCUCCGAACGUGUCACUCAACAUCAGUCUGAUAAGCUA-3′

negative control RNA, antisense:

5′-UCAGACUGAUGUUGAGUGACACGUUCGGAGAAGG-3′

miR-21: 5′-UAGCUUAUCAGACUGAUGUUGA-3′

single-base mismatched miR-21: 5′-UAGAUUAUCAGACUGAUGUUGA-3′

three-base mismatched miR-21: 5′-UAUCUUAGCAGACUCAUGUUGA-3′

miR-145: 5′-GUCCAGUUUUCCCAGGAAUCCCU-3′

The mismatched bases are underlined. All of the DNA were synthesized and purified by Sangon Biotech Co., Ltd. (Shanghai, China). Their sequences are listed in Table S1.

Apparatus. Absorption spectra were recorded on an UV-3600 UV−vis-NIR spectrophotometer (Shimadzu Company, Japan). The gel electrophoresis was performed on a DYCP-31BN Electrophoresis Analyzer (Liuyi Instrument Company, China) and imaged on Biorad ChemDoc XRS (Bio-Rad, USA). Fluorescence spectra were measured on an F-7000 spectrometer (HITACHI, Japan). Confocal fluorescence imaging of cells was performed on a TCS SP5 confocal laser scanning microscope (Leica, Ger-many). Flow cytometric analysis was performed on a Coulter FC-500 flow cytometer (Beckman-Coulter). Real-time reverse transcription polymerase chain reaction (RT-PCR) was performed on a StepOneTM RT-PCR detection system (Applied Biosystems, USA). MTT and ELISA assays were carried out on Hitachi/Roche System Cobas 6000 (680, Bio-Rad, USA). AFM imaging was performed under ambient conditions with an Agilent 5500 AFM/SPM system (USA). Dynamic light scattering measurements were performed on a 90 Plus/BI-MAS equipment (Brook haven, USA). Infrared (IR) spectra were acquired on a Nicolet NEXUS870 Fourier transform infrared (FT-IR) spectrometer (Madison, WI). Zeta potential analysis was performed on Zetasizer (Nano-Z, Malvern, UK). ^{1}H NMR spectra were recorded with a Bruker 500 MHz spectrometer.

Preparation of DNA Cycle. 4.2 μL of 100 μM phosphorylated linear DNA and 4.2 μL of 100 μM ligation DNA were mixed to anneal at 95 °C for 4 min. After the mixture was cooled to room temperature over 2 h, 1 μL of T4 DNA ligase (400 U/μL), 2 μL of 10 × T4 DNA buffer, and 8.6 μL ultrapure water were added, and the solution was incubated at 25 °C for 16 h. After T4 DNA ligase was inactivated by heating at 65 °C for 10 min, 4 μL of exonuclease I (20 U/μL) and 4 μL of exonuclease III (100 U/μL) were added, respectively, and the mixture was then incubated at 37 °C for 8 h to degrade ligation DNA. Afterward, the mixture was heated at 80 °C for 15 min to denature the exonuclease I and exonuclease III. The generated DNA cycle was stored at 4 °C before use.

Preparation of DNA Scaffold. The DNA scaffold was synthesized by rolling circle amplification (RCA).[51] 10 μL of 3 μM DNA cycle-8 and 0.5 μL of 100 μM DNA primer were mixed and annealed at 95 °C for 4 min. The mixture was slowly cooled to room temperature over 2 h and incubated with phi29 DNA polymerase (0.2 U/μL), BSA (0.4 μg/μL), and dNTPs (0.1 mM) at 37 °C for 5 h in 150 μL of 1 × phi29 reaction buffer. After RCA reaction, the mixture was incubated at 65 °C for 10 min to denature the phi29 DNA polymerase, then purified by DNA purification kit to obtain the DNA scaffold.

As controls, a series of DNMs with different numbers of bases between DR and D′R′ were prepared with DNA cycle-4, DNA cycle-8, DNA cycle-12, and DNA cycle-16 as components, respectively.

DOI: 10.1021/acsnano.8b02403
ACS Nano 2018, 12, 10797−10806

Preparation of DNM. DR and D′R′ were synthesized by mixing the stoichiometric amounts of D and Cy3-R (D′ and R′), respectively, at a final concentration of 10 μM in PBS buffer. The resulting solutions were heated to 95 °C for 5 min and slowly (1 °C/min) cooled down to room temperature. Twenty-five μL of 10 μM DR, 25 μL of 10 μM D′R′, and 300 μL of DNA scaffold were mixed together for 2 h at 37 °C to hybridize DR and D′R′ to DNA scaffold for the synthesis of DNM. The synthesized DNM was purified by ultrafiltration (100,000 MW cutoff membrane, Millipore) for three times.

To measure the amounts of DR and D′R′ in purified DNM, aminomethylcoumarin (AMCA)-labeled DNA primer (AMCA-DNA primer), Cy3-R, and Cy5-labeled R′ (Cy5-R′) were used as components to synthesize a tricolor DNM. From the fluorescence intensities of three dyes in DNM and the standard calibration curves for AMCA-DNA primer, Cy3-R, and Cy5-R′, their amounts could be obtained.

As controls, NR-DNM that was not responsive to miR-21 was synthesized by using Cy3-NR, R′, D, and D′ as components to hybridize with DNA scaffold, FR-DNM that could not generate siRNA was synthesized by hybridizing D and D′ with DNA scaffold, and NC-DNM that could generate control siRNA was synthesized by using negative control RNA, ND and ND′ as components to hybridize with DNA scaffold under the same conditions as DNM synthesis.

Polyacrylamide Gel Electrophoresis (PAGE) Analysis. 8% native polyacrylamide gel was prepared using 1 × TBE buffer. The loading samples were prepared by mixing 7 μL DNA samples, 1.5 μL 6 × loading buffer, and 1.5 μL UltraPowerTM dye and placed for 3 min before injected into polyacrylamide gel. The gel electrophoresis was run at 90 V for 60 min in 1 × TBE buffer and scanned with a Molecular Imager Gel Doc XR.

The intensity of the bands in the gel images was measured using Adobe Photoshop software. The sum intensity of each band represents the total amount of the DNA sample, which was used to calculate the siRNA generation efficiency of miRNA-triggered DNM.

AFM Imaging. Six μL sample was deposited on freshly cleaved mica surface and incubated for 2 min. After the solvent water was absorbed with filter paper, 20 μL ultrapure water was twice added to wash the mica. The mica was then dried with a nitrogen flow and scanned in tapping mode.

Serum Stability Assay of DNM. To verify the serum stability of DNM, Cy3 was tagged to R, and black hole quencher (BHQ2) was tagged to D for the preparation of self-quenched DNA/RNA hybrids (SQ-DR) and the assembly of self-quenched DNM (SQ-DNM). The SQ-DNM and SQ-DR were separately diluted to 100 nM with PBS containing 10% fetal bovine serum (FBS) and then incubated at 37 °C for 12 h. During this process, the Cy3 fluorescence was measured with 510 nm excitation and 560 nm emission. The fluorescence from Cy3 was quenched at the beginning due to the close distance between Cy3 and BHQ2.

Thermal Stability Assay of DNM. The sample for thermal stability assay was prepared by mixing 19 μL of 1 μM DNM solution with 1 μL of 20 × SYBR Green I in 0.2 mL PCR tubes (white). The fluorescence data at temperatures increasing from 30 to 90 °C at 0.2 °C/s and holding for 15 s in every measurement point were measured to obtain the melting curves.[48]

***In Vitro* SiRNA Generation.** To assess the *in vitro* generation of miR-21 controlled siRNA, 6 μL of miR-21 with various concentrations was added to 54 μL of 100 nM SQ-DNM solution to incubate at 37 °C for 60 min, respectively. The resulting mixtures were immediately subjected to fluorescence measurements. Fluorescence spectra were recorded with excitation at 510 nm. The slit width was set as 5 nm for the excitation and 5 nm for the emission. The *in vitro* siRNA generation was also performed by mixing 54 μL of 100 nM SQ-DR and 100 nM D′R′ with 6 μL miR-21 at various concentrations to incubate under the same condition for comparing the generation efficiency.

For FRET measurements, tetramethylrhodamine (TAMRA)-labeled R and 5-carboxyfluorescein (FAM)-labeled R′ were used as components to assemble bicolor DNM. The fluorescence spectra were recorded with excitation at 488 nm and the excitation and emission slit widths of 5 nm.

Preparation of Folic Acid Modified Polyethylenimine (FPEI). After EDC (10 mg) and NHS (20 mg) were mixed with 20 mL of saturated folic acid (0.0016 mg/mL) to react at room temperature for 40 min, polyethylenimine (PEI) solution (5 mL, 1 mg/mL) was injected into the mixture to incubate at room temperature for 48 h with stirring. The reaction product was purified through dialysis with a membrane (MWCO: 7,000) for 6 days and then freeze-dried under vacuum to obtain FPEI.

Assembly of DNM/FPEI. Purified DNM or SQ-DNM was mixed with FPEI at an N/P ratio of 10 and incubated at room temperature for 20 min. The resulting nanocomposite was further diluted with PBS (pH 7.4) to 100 nM for characterization and cell experiments.

As controls, NC-DNM/FPEI, NR-DNM/FPEI, and FR-DNM/FPEI nanocomposites were assembled by using NC-DNM, NR-DNM, and FR-DNM instead of DNM, respectively.

Cell Culture. Human cervix carcinoma (HeLa) cells (KeyGEN Biotech, Nanjing, China) were cultured in Dulbecco's modified Eagle's medium (DMEM) supplemented with 10% FBS, 100 μg/mL streptomycin, and 100 U/mL penicillin-streptomycin at 37 °C in a humidified incubator containing 5% CO_2 and 95% air. STR profiling and mycoplasma testing were conducted for each cell line before use. Cell numbers were determined with a Petroff-Hausser cell counter (USA).

Confocal Fluorescence Imaging and Flow Cytometric Assay. One $\times 10^4$ HeLa cells were seeded in a confocal dish and incubated in culture medium for 24 h at 37 °C. The medium was then replaced with 200 μL fresh culture medium containing 100 nM SQ-DNM/FPEI and incubated at 37 °C for 3 h. After washing twice with PBS, the fluorescence of cells was visualized from 550 to 610 nm on the confocal laser scanning microscope with the excitation wavelength of 514 nm for Cy3. All images were digitized and analyzed with the Leica Application Suite Advanced Fluorescence (LAS-AF) software package. The flow cytometric assay was performed in PBS with FL2 channel.

For nuclear localization imaging, HeLa cells were incubated with 100 nM SQ-DNM/FPEI for 3 h followed by staining with 5 μg/mL DAPI for 10 min. DAPI was excited at 405 nm, and the fluorescence signal was collected from 450 to 500 nm.

Endocytosis Pathway of DNM/FPEI. The endocytosis pathway was examined as follows: After HeLa cells were seeded in confocal dishes *via* 24 h incubation, 450 mM sucrose, 200 μg/mL genistein, 50 nM wortmannin, and 10 mM NaN_3 as uptake inhibitors were added into different cell-adhered dishes to inhibit clathrin, caveolae, macropinocytosis, and energy-dependent endocytosis, respectively.[48,49] After incubation for 30 min at 37 °C, these cells were loaded with SQ-DNM/FPEI nanocomposite, during which the inhibitors were maintained, to perform the flow cytometric analysis for measuring the uptake amount of SQ-DNM/FPEI.

MTT Assay. HeLa cells were seeded into two 96-well plates (5×10^5 per well) and incubated in 200 μL culture medium for 24 h at 37 °C. The cells were then washed with PBS and incubated with serial concentrations of DNM/FPEI for 3 h. As controls, FPEI, NR-DNM/FPEI, FR-DNM/FPEI, and NC-DNM/FPEI were incubated with HeLa cells under the same conditions. After these cells were washed twice with PBS, 50 μL of 5 mg/mL MTT solution was added to incubate for 4 h. Afterward, the medium was removed, and 150 μL of DMSO was added to dissolve the formazan crystal precipitates. After shaking the cell plate for 15 min, the optical density (OD) at a wavelength of 490 nm was measured with a Bio-Rad microplate reader. The relative cell viability (%) was calculated by $(A_{test}/A_{control}) \times 100\%$.

Gene Silencing Assay. HeLa cells were seeded into 24-well plate at 5×10^5 per well and incubated for 24 h at 37 °C. After the cells were washed with PBS, 100 nM of DNM/FPEI was added to incubate for 3 h at 37 °C. Meanwhile, FPEI, NC-DNM/FPEI, NR-DNM/FPEI, and FR-DNM/FPEI were incubated with HeLa cells under the same condition as controls. After the medium was replaced by a fresh

DOI: 10.1021/acsnano.8b02403
ACS Nano 2018, 12, 10797−10806

culture medium containing 10% FBS and further cultured for 48 h, the supernatant of culture medium was collected and analyzed by ELISA to quantify VEGF secreted from the cells. Total RNAs from the transfected HeLa cells were extracted using Trizol reagent (Invitrogen, USA), and cDNA of VEGF was generated using PrimeScriptRT reagent kit (Takara). The cDNA was detected with real-time PCR (RT-PCR) to calculate the level of cellular VEGF mRNA.

Cell Apoptosis Experiments. After 5.0×10^5 HeLa cells were seeded in a 24-well plate for 24 h at 37 °C, they were incubated with 200 μL culture medium containing 100 nM DNM/FPEI or FPEI, NC-DNM/FPEI, NR-DNM/FPEI, and FR-DNM/FPEI as controls for 3 h at 37 °C. The cells were further incubated for 48 h after the supernatant medium was replaced with fresh culture medium containing 10% FBS. The cells were then collected and stained with the mixture of 5.0 μL Annexin V-FITC and 5.0 μL propidium iodide (PI) for 15 min and analyzed with flow cytometry over FL1 (Annexin V-FITC) and FL3 (PI) channels. Similar procedures were also performed for HepG2 cells to verify the therapeutic efficiency of the DNM/FPEI in other cancers.

To compare the therapeutic efficiencies for DNM and the mixture of DR and D′R′, MTT assay, gene silencing assay, and cell apoptosis experiments were conducted according to the above procedures except that HeLa cells were treated with the mixture of Lipofectamine 2000 (0.5 μL) and DNM (100 nM, 200 μL) or the mixture of Lipofectamine 2000 (0.5 μL) and DR/D′R′ (200 nM, 100 μL) for 3 h at 37 °C.

***In Vivo* Antitumor Efficacy.** All animals were treated in according with institutional animal use and care regulations approved by the Jiangsu Simcere Pharmaceutical Research Institute, which allowed the maximal diameter (length) of every tumor to not exceed 20 mm or the volume of every tumor to be <2.0 cm^3. Specific pathogen-free female BALB/c nude mice (5−6 weeks of age) were purchased from Shanghai Laboratory Animal Center, Chinese Academy of Sciences, and bred in an axenic environment. To set up a HeLa tumor model, 1.0×10^6 HeLa cells were subcutaneous injected into the selected position of the nude mice. When the tumor volumes reached to 75 mm^3, the mice were randomly divided into four groups and intravenously injected with 50 μL PBS, DNM/FPEI, NC-DNM/FPEI, and NR-DNM/FPEI at a dose of 500 pmol per mouse. The injections were performed every other day for five times, and meanwhile the tumor sizes were measured every 2 days by a digital caliper for 14 days. The tumor volumes were calculated as $V = (L \times W^2)/2$, where L and W are the length and width of the tumor, respectively.

ASSOCIATED CONTENT

Supporting Information

The Supporting Information is available free of charge on the ACS Publications website at DOI: 10.1021/acsnano.8b02403.

Evaluation of DR/D′R′ numbers assembled in DNM; characterization of DNM stability; characterization of FPEI synthesis and DNM/FPEI assembly; specificity evaluation miRNA-triggered siRNA assembly; effect of the distance between DR and D′R′ in SQ-DNM on siRNA generation efficiency; kinetic analysis of miRNA-triggered siRNA assembly; z-stack images of HeLa cells; nuclear localization images; RT-PCR analysis of miR-21 in HeLa cells; characterization of siRNA assembly in HeLa cells; characterization of DNM/FPEI delivery specificity and its endocytosis pathways; HeLa cell proliferation assay; comparison of therapeutic efficiencies in presence and absence of DNA scaffold; characterization of siRNA assembly and therapeutic effect of DNM/FPEI in HepG2 cells; body weight variation of mice; and sequences of oligonucleotides (PDF)

AUTHOR INFORMATION

Corresponding Authors

*E-mail: yingliu@nju.edu.cn.
*E-mail: hxju@nju.edu.cn.

ORCID

Yue Zhang: 0000-0002-7902-4253
Ying Liu: 0000-0001-5718-7804
Huangxian Ju: 0000-0002-6741-5302

Author Contributions

§These authors contributed equally.

Notes

The authors declare no competing financial interest.

ACKNOWLEDGMENTS

We gratefully acknowledge National Natural Science Foundation of China (21605083, 21635005, 21361162002), Natural Science Foundation of Jiangsu Province (BK20160644), and the National Research Foundation for Thousand Youth Talents Plan of China.

REFERENCES

(1) Yu, D.; Pendergraff, H.; Liu, J.; Kordasiewicz, H. B.; Cleveland, D. W.; Swayze, E. E.; Lima, W. F.; Crooke, S. T.; Prakash, T. P.; Corey, D. R. Single-Stranded RNAs Use RNAi to Potently and Allele-Selectively Inhibit Mutant Huntingtin Expression. *Cell* **2012**, *150*, 895−908.

(2) Shi, J. J.; Kantoff, P. W.; Wooster, R.; Farokhzad, O. C. Cancer Nanomedicine: Progress, Challenges and Opportunities. *Nat. Rev. Cancer* **2017**, *17*, 20−37.

(3) Castanotto, D.; Rossi, J. J. The Promises and Pitfalls of RNA-Interference-Based Therapeutics. *Nature* **2009**, *457*, 426−433.

(4) Liu, Y. L.; Gunda, V.; Zhu, X.; Xu, X. D.; Wu, J.; Askhatova, D.; Farokhzad, O. C.; Parangi, S.; Shi, J. J. Theranostic Near-infrared Fluorescent Nanoplatform for Imaging and Systemic SiRNA Delivery to Metastatic Anaplastic Thyroid Cancer. *Proc. Natl. Acad. Sci. U. S. A.* **2016**, *113*, 7750−7775.

(5) Castleberry, S.; Wang, M.; Hammond, P. T. Nanolayered SiRNA Dressing for Sustained Localized Knockdown. *ACS Nano* **2013**, *7*, 5251−5261.

(6) Whitehead, K. A.; Langer, R.; Anderson, D. G. Knocking Down Barriers: Advances in SiRNA Delivery. *Nat. Rev. Drug Discovery* **2009**, *8*, 129−138.

(7) Khvorova, A.; Watts, J. K. The Chemical Evolution of Oligonucleotide Therapies of Clinical Utility. *Nat. Biotechnol.* **2017**, *35*, 238−248.

(8) Conde, J.; Oliva, N.; Atilano, M.; Song, H. S.; Artzi, N. Self-Assembled RNA-Triple-Helix Hydrogel Scaffold for MicroRNA Modulation in the Tumour Microenvironment. *Nat. Mater.* **2016**, *15*, 353−363.

(9) Won, Y. W.; Adhikary, P. P.; Lim, K. S.; Kim, H. J.; Kim, J. K.; Kim, Y. H. Oligopeptide Complex for Targeted Non-Viral Gene Delivery to Adipocytes. *Nat. Mater.* **2014**, *13*, 1157−1164.

(10) Jang, M.; Kim, J. H.; Nam, H. Y.; Kwon, I. C.; Ahn, H. J. Design of a Platform Technology for Systemic Delivery of SiRNA to Tumours Using Rolling Circle Transcription. *Nat. Commun.* **2015**, *6*, 7930.

(11) Pelaz, B.; Alexiou, C. H.; Alvarez-Puebla, R. A.; Alves, F.; Andrews, A. M.; Ashraf, S.; Balogh, L. P.; Ballerini, L.; Bestetti, A.; Brendel, C.; Bosi, S.; Carril, M.; Chan, W. C. W.; Chen, C. Y.; Chen, X. D.; Chen, X. Y.; Cheng, Z.; Cui, D. X.; Du, J. Z.; Dullin, C.; et al. Diverse Applications of Nanomedicine. *ACS Nano* **2017**, *11*, 2313−2381.

(12) Roh, Y. H.; Deng, J. Z.; Dreaden, E. C.; Park, J. H.; Yun, D. S.; Shopsowitz, K. E.; Hammond, P. T. A Multi-RNAi Microsponge

DOI: 10.1021/acsnano.8b02403
ACS Nano 2018, 12, 10797−10806

Platform For Simultaneocs Controlled Delivery Of Multiple Small Interfering RNAs. *Angew. Chem., Int. Ed.* **2016**, *55*, 3347−3351.
(13) Wang, Y.; Kohane, D. S. External Triggering and Triggered Targeting Strategies for Drug Delivery. *Nat. Rev. Mater.* **2017**, *2*, 17020.
(14) Karimi, M.; Ghasemi, A.; Sahandi Zangabad, P.; Rahighi, R.; Moosavi Basri, S. M.; Mirshekari, H.; Amiri, M.; Shafaei Pishabad, Z.; Aslani, A.; Bozorgomid, M.; Ghosh, D.; Beyzavi, A.; Vaseghi, A.; Aref, A. R.; Haghani, L.; Bahrami, S.; Hamblin, M. R. Smart Micro/Nanoparticles in Stimulus-Responsive Drug/Gene Delivery Systems. *Chem. Soc. Rev.* **2016**, *45*, 1457−1501.
(15) Groves, B.; Chen, Y. J.; Zurla, C.; Pochekailov, S.; Kirschman, J. L.; Santangelo, P. J.; Seelig, G. Computing in Mammalian Cells with Nucleic Acid Strand Exchange. *Nat. Nanotechnol.* **2016**, *11*, 287−294.
(16) Afonin, K. A.; Viard, M.; Martins, A. N.; Lockett, S. J.; Maciag, A. E.; Freed, E. O.; Heldman, E.; Jaeger, L.; Blumenthal, R.; Shapiro, B. A. Activation of Different Split Functionalities on Re-Association of RNA-DNA Hybrids. *Nat. Nanotechnol.* **2013**, *8*, 296−304.
(17) Li, J.; Green, A. A.; Yan, H.; Fan, C. Engineering Nucleic Acid Structures for Programmable Molecular Circuitry and Intracellular Biocomputation. *Nat. Chem.* **2017**, *9*, 1056−1067.
(18) Bar-Ziv, R. Materials Science. DNA Circuits Get up to Speed. *Science* **2007**, *318*, 1078−1079.
(19) Stoeger, T.; Battich, N.; Pelkmans, L. Passive Noise Filtering by Cellular Compartmentalization. *Cell* **2016**, *164*, 1151−1161.
(20) Thubagere, A. J.; Li, W.; Johnson, R. F.; Chen, Z.; Doroudi, S.; Lee, Y. L.; Izatt, G.; Wittman, S.; Srinivas, N.; Woods, D.; Winfree, E.; Qian, L. A Cargo-Sorting DNA Robot. *Science* **2017**, *357*, eaan6558.
(21) Adamala, K. P.; Martin-Alarcon, D. A.; Guthrie-Honea, K. R.; Boyden, E. S. Engineering Genetic Circuit Interactions within and between Synthetic Minimal Cells. *Nat. Chem.* **2017**, *9*, 431−439.
(22) Surana, S.; Bhat, J. M.; Koushika, S. P.; Krishnan, Y. An Autonomous DNA Nanomachine Maps Spatiotemporal pH Changes in a Multicellular Living Organism. *Nat. Commun.* **2011**, *2*, 340.
(23) Clayden, J. Supramolecular Chemistry: Host in Translation. *Nat. Nanotechnol.* **2017**, *12*, 403−404.
(24) Linko, V.; Eerikainen, M.; Kostiainen, M. A. A Modular DNA Origami-Based Enzyme Cascade Nanoreactor. *Chem. Commun.* **2015**, *51*, 5351−5354.
(25) Zhao, Z.; Fu, J.; Dhakal, S.; Johnson-Buck, A.; Liu, M.; Zhang, T.; Woodbury, N. W.; Liu, Y.; Walter, N. G.; Yan, H. Nanocaged Enzymes with Enhanced Catalytic Activity and Increased Stability against Protease Digestion. *Nat. Commun.* **2016**, *7*, 10619.
(26) Fu, J.; Yang, Y. R.; Johnson-Buck, A.; Liu, M.; Liu, Y.; Walter, N. G.; Woodbury, N. W.; Yan, H. Multi-Enzyme Complexes on DNA Scaffolds Capable of Substrate Channelling with an Artificial Swinging Arm. *Nat. Nanotechnol.* **2014**, *9*, 531−536.
(27) Niu, J.; Hili, R.; Liu, D. R. Enzyme-Free Translation of DNA into Sequence-Defined Synthetic Polymers Structurally Unrelated to Nucleic Acids. *Nat. Chem.* **2013**, *5*, 282−292.
(28) Meng, W.; Muscat, R. A.; McKee, M. L.; Milnes, P. J.; El-Sagheer, A. H.; Bath, J.; Davis, B. G.; Brown, T.; O'Reilly, R. K.; Turberfield, A. J. An Autonomous Molecular Assembler for Programmable Chemical Synthesis. *Nat. Chem.* **2016**, *8*, 542−548.
(29) He, Y.; Liu, D. R. Autonomous Multistep Organic Synthesis in a Single Isothermal Solution Mediated by a DNA Walker. *Nat. Nanotechnol.* **2010**, *5*, 778−782.
(30) McKee, M. L.; Milnes, P. J.; Bath, J.; Stulz, E.; O'Reilly, R. K.; Turberfield, A. J. Programmable One-Pot Multistep Organic Synthesis Using DNA Junctions. *J. Am. Chem. Soc.* **2012**, *134*, 1446−1449.
(31) Wheeldon, I.; Minteer, S. D.; Banta, S.; Barton, S. C.; Atanassov, P.; Sigman, M. Substrate Channelling as an Approach to Cascade Reactions. *Nat. Chem.* **2016**, *8*, 299−309.
(32) Küchler, A.; Yoshimoto, M.; Luginbühl, S.; Mavelli, F.; Walde, P. Enzymatic Reactions in Confined Environments. *Nat. Nanotechnol.* **2016**, *11*, 409−420.
(33) Chatterjee, G.; Dalchau, N.; Muscat, R. A.; Phillips, A.; Seelig, G. A Spatially Localized Architecture for Fast and Modular DNA Computing. *Nat. Nanotechnol.* **2017**, *12*, 920−927.
(34) Liang, C.-P.; Ma, P.-Q.; Liu, H.; Guo, X.; Yin, B.-C.; Ye, B.-C. Rational Engineering of a Dynamic, Entropy-Driven DNA Nanomachine for Intracellular MicroRNA Imaging. *Angew. Chem., Int. Ed.* **2017**, *56*, 9077−9081.
(35) Dowdy, S. F. Overcoming Cellular Barriers for RNA Therapeutics. *Nat. Biotechnol.* **2017**, *35*, 222−229.
(36) Wittrup, A.; Lieberman, J. Knocking Down Disease: A Progress Report on siRNA Therapeutics. *Nat. Rev. Genet.* **2015**, *16*, 543−552.
(37) Volker, J.; Klump, H. H.; Breslauer, K. J. DNA Energy Landscapes *Via* Calorimetric Detection of Microstate Ensembles of Metastable Macrostates and Triplet Repeat Diseases. *Proc. Natl. Acad. Sci. U. S. A.* **2008**, *105*, 18326−18330.
(38) Seelig, G.; Yurke, B.; Winfree, E. Catalyzed Relaxation of a Metastable DNA Fuel. *J. Am. Chem. Soc.* **2006**, *128*, 12211−12220.
(39) Xing, Y.; Yang, Z.; Liu, D. A Responsive Hidden Toehold to Enable Controllable DNA Strand Displacement Reactions. *Angew. Chem., Int. Ed.* **2011**, *50*, 11934−11936.
(40) Sun, W.; Ji, W.; Hall, J. M.; Hu, Q.; Wang, C.; Beisel, C. L.; Gu, Z. Self-Assembled DNA Nanoclews for the Efficient Delivery of CRISPR-Cas9 for Genome Editing. *Angew. Chem., Int. Ed.* **2015**, *54*, 12029−12033.
(41) Deng, R.; Tang, L.; Tian, Q.; Wang, Y.; Lin, L.; Li, J. Toehold-Initiated Rolling Circle Amplification for Visualizing Individual MicroRNAs *in Situ* in Single Cells. *Angew. Chem., Int. Ed.* **2014**, *53*, 2389−2393.
(42) Lv, Y.; Hu, R.; Zhu, G.; Zhang, X.; Mei, L.; Liu, Q.; Qiu, L.; Wu, C.; Tan, W. Preparation and Biomedical Applications of Programmable and Multifunctional DNA Nanoflowers. *Nat. Protoc.* **2015**, *10*, 1508−1524.
(43) Lau, K. L.; Hamblin, G. D.; Sleiman, H. F. Gold Nanoparticle 3D-DNA Building Blocks: High Purity Preparation and Use for Modular Access to Nanoparticle Assemblies. *Small* **2014**, *10*, 660−666.
(44) Mok, H.; Lee, S. H.; Park, J. W.; Park, T. G. Multimeric Small Interfering Ribonucleic Acid for Highly Efficient Sequence-Specific Gene Silencing. *Nat. Mater.* **2010**, *9*, 272−278.
(45) Lee, S. J.; Huh, M. S.; Lee, S. Y.; Min, S.; Lee, S.; Koo, H.; Chu, J. U.; Lee, K. E.; Jeon, H.; Choi, Y.; Choi, K.; Byun, Y.; Jeong, S. Y.; Park, K.; Kim, K.; Kwon, I. C. Tumor-Homing Poly-SiRNA/Glycol Chitosan Self-Cross-Linked Nanoparticles for Systemic SiRNA Delivery in Cancer Treatment. *Angew. Chem., Int. Ed.* **2012**, *51*, 7203−7207.
(46) Wu, P.; Hwang, K.; Lan, T.; Lu, Y. A DNAzyme-Gold Nanoparticle Probe for Uranyl Ion in Living Cells. *J. Am. Chem. Soc.* **2013**, *135*, 5254−5257.
(47) Yang, Y.; Huang, J.; Yang, X.; Quan, K.; Wang, H.; Ying, L.; Xie, N.; Ou, M.; Wang, K. FRET Nanoflares for Intracellular mRNA Detection: Avoiding False Positive Signals and Minimizing Effects of System Fluctuations. *J. Am. Chem. Soc.* **2015**, *137*, 8340−8343.
(48) Ohta, S.; Glancy, D.; Chan, W. C. W. DNA-Controlled Dynamic Colloidal Nanoparticle Systems For Mediating Cellular Interaction. *Science* **2016**, *351*, 841−845.
(49) Chen, G.; Liu, D.; He, C.; Gannett, T. R.; Lin, W.; Weizmann, Y. Enzymatic Synthesis of Periodic DNA Nanoribbons for Intracellular pH Sensing and Gene Silencing. *J. Am. Chem. Soc.* **2015**, *137*, 3844−3851.
(50) Liang, L.; Li, J.; Li, Q.; Huang, Q.; Shi, J.; Yan, H.; Fan, C. Single-Particle Tracking and Modulation of Cell Entry Pathways of a Tetrahedral DNA Nanostructure in Live Cells. *Angew. Chem., Int. Ed.* **2014**, *53*, 7745−7750.
(51) Han, D.; Wu, C.; You, M.; Zhang, T.; Wan, S.; Chen, T.; Qiu, L.; Zheng, Z.; Liang, H.; Tan, W. A Cascade Reaction Network Mimicking the Basic Functional Steps of Adaptive Immune Response. *Nat. Chem.* **2015**, *7*, 835−841.

DOI: 10.1021/acsnano.8b02403
ACS Nano 2018, 12, 10797−10806